

Photometric and astrometric vagaries of the enigma star KIC 8462852

Valeri V. Makarov

vvm@usno.navy.mil

US Naval Observatory, 3450 Massachusetts Ave NW, Washington DC 20392-5420, USA

Alexey Goldin

alexey.goldin@gmail.com

Teza Technology, 150 N Michigan Ave, Chicago IL 60601, USA

Accepted . Received ; in original form

ABSTRACT

We apply a PCA-based pre-whitening method to the entire collection of main Kepler mission long-cadence data for KIC 8462852 spanning four years. This technique removes the correlated variations of instrumental origin in both the detected light curves and astrometry, resolving intrinsic changes in flux and image position of less than 100 ppm and 1 mas, respectively. Beside the major dips in the light curve during mission quarters 8 and 16, when the flux dropped by up to 20%, we confirm multiple smaller dips across the time span of observation with amplitudes ranging from 0.1% to 7%. A variation of flux with a period of 0.88 d and a half-amplitude of approximately 90 ppm is confirmed in the PCA-cleaned data. We find that the phase of the wave is steady over the entire 15-month interval. We confidently detect a weak variability-induced motion (VIM) effect in the cleaned astrometric trajectories, when the moment-based centroids shift synchronously with the flux dips by up to 0.0008 pixels on the detector. The inconsistent magnitude and direction of VIM effects within the same quarter point at more than one source of photometric variability in the blended image. The 0.88 d periodicity comes from a different source, not from the target star KIC 8462852. We discuss a possible interpretation of the bizarre properties of the source as a swarm of interstellar junk (comets and planetoids) crossing the line of sight to the star and its optical companions at approximately 7 mas per year.

1. Introduction

The star KIC 8462852 = TYC 3162-665-1, with unique and strange photometric features in the Kepler long-cadence light curves, was serendipitously discovered by the Planet Hunters

team (Boyajian et al. 2016) who routinely inspected thousands of targets with candidate exoplanet transit events. The star underwent a series of dimming events during the 4 years of nominal Kepler mission of variable depth and duration, ranging from ~ 1000 parts per million (ppm) in relative flux to $\sim 210\,000$ ppm. The most unusual features of these events are the apparent lack of periodicity and repeatability and asymmetry of their shape. The discoverers collected follow-up observations of the star, including spectroscopic and radial velocity measurements and high-resolution imaging and speckle interferometry. These additional data allowed the authors to rule out a number of hypotheses, such as a double star, a very young star with stochastic variability, and an evolved supergiant of the R Coronae Borealis type. A system of large comets on highly eccentric orbits or dust and rock debris resulting from a catastrophic collision of planets emerged as the likeliest explanation. However, neither infrared (Marengo et al. 2015) nor submillimetre (Thompson et al. 2016) continuum fluxes show any significant excess, practically disproving the presence of dusty material around the star. Somewhat heuristically, artificial manipulation of the stellar irradiation by an extraterrestrial intelligence has been proposed, and efforts to detect other signals or signs of such an activity have been made (Abeysekara et al. 2016). The characteristics of the detected photometric events may be consistent with occultations by giant artificial megastructures (Wright et al. 2016).

In this paper, we revisit the data collected by the Kepler main mission for KIC 8462852 and for other stars observed on the same CCD detectors as this star. Our aim is to contribute to the in-depth analysis of Kepler data with the following updates in the approach.

- We use the raw Simple Aperture Photometry (SAP) light curves as opposed to the Pre-search Data Conditioning (PDC) fluxes derived by the data processing pipeline (Christiansen et al. 2012). The de-trending procedures that fit low-order polynomials to remove the slow variations of flux in the raw data are not always sufficient to mitigate the common instrumental perturbations shared by targets on the same channel, and can in fact distort the light curve on time scales longer than a few days. Be mindful that the main purpose of PDC was to provide the most reliable information about possible exoplanet transits, likely at some expense to longer-term variability.
- To remove most of the correlated perturbation of instrumental origin common to all targets within a given CCD channel, we design and apply an ad hoc pre-whitening technique based on Principal Component Analysis (PCA). The method is described in Sect. 2. This allows us to come as close as possible to the intrinsic variability of the star at a level of 20 ppm and for time scales up to 90 days after removing the much greater detrimental variations of instrumental origin.
- For the first time, we analyze in detail the astrometric data gathered by Kepler, i.e., the photocentre centroids measured at the same cadence and simultaneously with the flux. Synchronous astrometric excursions of centroids, called Variability Induced Motion (VIM), provide a powerful method of detecting double stars or other events of signal

blending (Makarov & Goldin 2016). VIM occurs when one of the blended sources in the aperture is photometrically variable. Since the recorded centroid corresponds to the first moment of the distribution of flux over the pixel grid, which is sensitive to the flux ratio of the blended components, the photocenter moves in a strongly correlated way with the total flux. The collection of Kepler long cadence data is full of VIM manifestations, many of the intended targets being blended with something else. Correlated excursions of instrumental origin due to pointing events, micrometeoroid strikes, etc., are efficiently removed or suppressed by the same pre-whitening technique with appropriate modifications. This allows us to detect genuine astrometric signals at a level ~ 0.0002 pixels, which corresponds to ~ 1 mas on the sky. A detailed study of the detected VIM signals for the star in question is given in Section 4.

- Using the least-squares Lomb periodogram, we analyze the sinusoidal signals in both the pre-whitened light curves and astrometric trajectories (Section 5). Using the data in quarters 9 through 13 when the star was the most quiescent the stability of the phase of the 0.88 d variation is evaluated.

Given the previously accumulated and newly obtained information, some conclusions and possible astrophysical interpretation of the highly unusual astrometric and photometric properties of KIC 8462852 are given in Section 6.

2. Pre-whitening based on PCA

A number of adverse instrumental effects can cause apparent motion of stellar images across the plane of detector. They include pointing shifts, gyroscope zero-point crossing, micrometeoroid strikes, etc. The resulting translational (drift) and rotational (roll) perturbation affects all stars within one CCD channel in very similar ways. Normally, each target was observed with a fixed digital aperture, or window, comprising a set of specific pixels. The shape and size of the aperture depend on the point spread function (PSF) and the configuration of near neighbors, maximizing the collected flux but minimizing blending with other sources. The Kepler telescope design was driven by the requirement to observe a large number of targets in a wide field of view almost uninterruptedly. The Schmidt design with a corrector plate and a mosaic field flattener provides the required field, but the optical quality of star images is uncharacteristically low for a space telescope. The wide and often distinctly asymmetric PSF spills over the edges of the digital aperture, and any motion of the photocentre with respect to the grid of pixels results in variations in both the aperture flux and the calculated flux-weighted centroid. Due to the very high sensitivity and relative precision of Kepler measurements, even small amounts of drift or roll result in correlated changes in the recorded flux and centroids of targets that are situated close to each other in the detector plane. Differential aberration

of starlight¹ within the wide field of view is another significant contributor to such correlated trends.

Let \mathbf{d}_i be a column vector comprising data of interest (for example, a light curve time-sequence) for star i . We can construct a data matrix \mathbf{D} consisting of vectors \mathbf{d}_i for a set of stars as long as the observations are on the same cadence, which is the case with the Kepler long-cadence data². The matrix $\mathbf{D} = (\mathbf{d}_1, \mathbf{d}_2, \dots, \mathbf{d}_n)$, where n is the number of objects, has a full rank n and a singular value decomposition (SVD, Golub & Van Loan (1983)):

$$\mathbf{U} \mathbf{\Sigma} \mathbf{V}^T = \mathbf{D}. \quad (1)$$

The matrices \mathbf{U} and \mathbf{V} comprise basis vectors in the space spanned by the columns and rows of \mathbf{D} , respectively. Only the columns of $\mathbf{U} = (\mathbf{u}_1, \mathbf{u}_2, \dots, \mathbf{u}_n)$, called the *principal components* of \mathbf{D} , are of interest for this analysis. $\mathbf{\Sigma}$ is a diagonal matrix comprising singular values $\sigma_1, \sigma_2, \dots, \sigma_n$, always in descending order by design, $\sigma_1 \geq \sigma_2 \geq \dots \geq \sigma_n$. Since the norm of the projection $\|\mathbf{D}^T \mathbf{u}_i\| = \mathbf{u}_i^T \mathbf{U} \mathbf{\Sigma} \mathbf{V}^T \mathbf{V} \mathbf{\Sigma} \mathbf{U}^T \mathbf{u}_i = \sigma_i^2$, for any i between 1 and n , the first singular vector \mathbf{u}_1 is the most significant principal component for the given set of data vectors, i.e., the best aligned with the data vectors, followed by \mathbf{u}_2 , \mathbf{u}_3 , etc., in decreasing significance. Any of the observations \mathbf{d}_i can be exactly represented as a linear combination of n singular vectors \mathbf{u}_i , but if we want to produce the closest and most faithful fit with a limited number of basis vectors, we should take the first ones. If the data vectors were all orthogonal (which never happens), the singular values would all be equal, and the singular vectors would have the same significance. If there is some degree of commonality in the data vectors, such as common trends, localized perturbations, etc., the first few singular vectors (or principal components) will represent them to the highest possible degree. This is essentially the justification of the PCA.

Our objective is to remove as much of the correlated trend in a time series as possible without distorting the genuine signal specific to a given object. De-correlation of data, which is sometimes called pre-whitening, can be achieved by removing the most significant principal components from it. The pre-whitened data vector is then

$$\hat{\mathbf{d}} = \mathbf{d} - \sum_{i=1}^k \alpha_i \mathbf{u}_i \quad (2)$$

where α_i are the direction cosines of \mathbf{d} in the subspace spanned by the first k singular basis vectors. Since the basis vectors \mathbf{u}_i are orthonormal, these coefficients are computed by direct projection rather than by a least-squares regression:

$$\alpha_i = \mathbf{u}_i^T \mathbf{d}. \quad (3)$$

¹The main part of stellar aberration was taken out by the active pointing control.

²In fact, the recorded times of observation may spread by ~ 0.144 min between stars on the same chip at the same readout, but this spread is negligible in the framework of this paper.

The technical implementation of this method is rather subtle, despite the seemingly simple principle. One of the crucial decisions, which potentially can greatly alter the result, is how to normalize the data vectors before computing the singular vectors and the principal components. Normalization is required, because bright stars with a large degree of intrinsic variability can get too much weight in the SVD, which defeats the purpose of pre-whitening. Our ad hoc method developed for this analysis is similar to the cotrending technique developed by Tom Barclay, realized as the `kepcotrend` subroutine in the PyKE contributed software package (Still & Barclay 2012). There are important differences in the implementation. The PyKE algorithm is based on principal components computed for only 50% of “most correlated” light curves observed within each CCD channel over a quarter. We consider it important to use as many data vectors as possible for the SVD, to minimize the influence of intrinsic photometric variability and reduce the level of noise in the principal components. Therefore, we are using all light curves collected within a given channel³. After the selection of most correlated data vectors, the PyKE algorithm does not apply any normalization for the final SVD, whereas we apply the required subtraction of the median flux followed by a minmax normalization bringing the range of variation to unity. This allows us to minimize the adverse impact of stars with very noisy data, large degrees of intrinsic variability, or occasional observational outliers. Finally, we apply the same number of first principal components for all batches of observations. It is hard to justify skipping some of the most significant components in favor of less significant ones, so the only choice in this case is how many of the components to use.

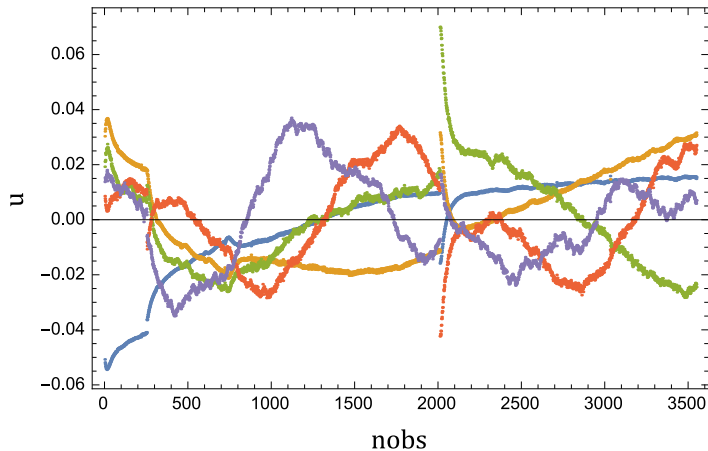


Fig. 1.— The first five principal components (basis vectors \mathbf{u}_i , $i = 1, 2, \dots, 5$) of the collection of 1828 light curves collected in Q16 on channel 56. Note that the components capture a common dip in the light curves at approximately $nobs = 2000$, which was probably due to a temporary misalignment of the telescope caused by a micrometeoroid hit.

The limiting number k was determined by experimenting with real Kepler light curves. We investigated in depth the properties of PCA and filtered data for one quarter, Q16, and all 1828

³It is not advisable to include data from other channels because the instrumental effects can differ for each particular chip.

stars observed in this quarter in channel 56. Our object of investigation, KIC 8462852, was also observed in this channel in Q16. The first 5 principal components for the collection of 1828 light curves are shown in Fig. 1. Note that the vectors are orthonormal by design, so they are dissimilar to one another to the highest degree. Generally, they display some smooth variations with time, but also capture some short-term adverse effects. After applying progressively greater numbers of principal components according to Eq. 2, and computing the 2-norm of residuals, we determined that the latter begins to be reduced by 1% or less with respect to the most significant component already when 4 principal components applied. Consequently, the filtered light curves with 5, 6, etc. components applied were hard to distinguish from the 4 PC-filtered curve by eye. The amount of high-frequency noise, which is present in the principal components in small amounts, on the other hand, grows roughly proportional to the number of PC used. Therefore, we found it nearly optimal to use 4 components throughout our analysis.

We also checked if a few stars with large degrees of variability can affect the first 4 principal components, a potentially harmful possibility which can bring about unintended consequences. Our scaling and normalization scheme turns out to be quite efficient in downweighting such extreme outliers. The first principal components do not display any features from the most variable data vectors, which are usually pulsating, eclipsing stars or artifacts. The same is true for the principal components of the x (column) and y (row) coordinates. For example, by far the largest variation in column pixel coordinates for the test sample, exceeding 2 pixels in magnitude, is found for the target KIC 8653134. These great excursions of the photocenter are artifacts caused by blending with some extraneous very bright signal, also observed in Q4 and Q8. Without the normalization of observed data by the standard deviation of the observed variation, this single data vector could have corrupted the computed principal components and damaged the PCA pre-whitening.

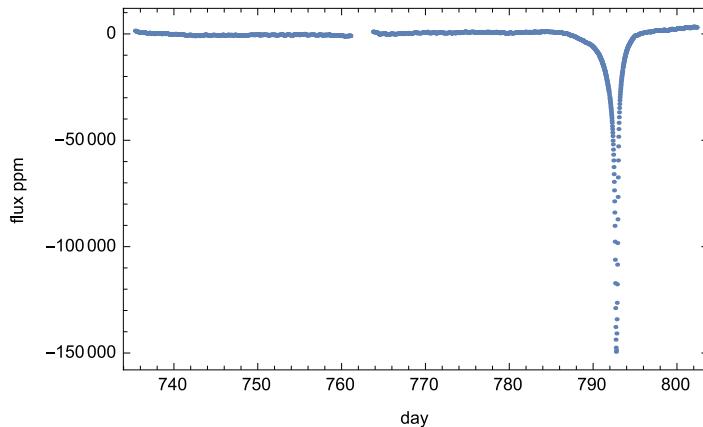


Fig. 2.— PCA-cleaned light curve of KIC 8462852 in Quarter 8 in relative units of ppm. The major flux dip on day 793 is one of the most prominent and unusual features of this dataset almost reaching 15%.

Another important difference with the PyKE implementation of the PCA is the way we

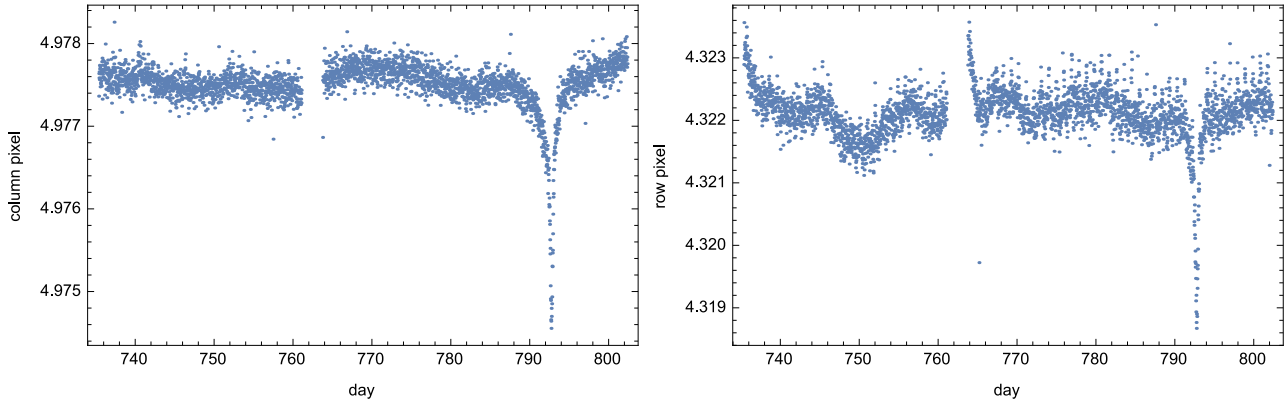


Fig. 3.— PCA-cleaned centroid trajectories of KIC 8462852 in Quarter 8 in column (left) and row (right) pixel coordinates. Note the clear VIM effect caused by the major flux dip on day 793 and the periodic motion in row pixels with 0.88 d period.

perform the fitting of the principal components to the data. Eq. 2 shows a simple projection of the data vector onto the null space of the first basis vectors. For many regular stars of moderate or small variability, this simple method works fine, but targets with powerful changes in the light curve, such as our target KIC 8462852, may require a more careful selection of the data points to fit. A single dip, such as the one on day 793, can push the fit giving too much weight to a basis vector that has a depression in this part of the time series. The PyKE PCA algorithm employs iterative filtering of data points deviating by more than a certain threshold amount from the fit in the preceding iteration (clipping of outliers). We chose a more advanced method of dealing with outliers, which we had successfully used in other analyses. Generally, a least-squares (LS) method heavily relies on the assumptions that are often not met in practice. In particular, it is assumed that data errors are normally distributed. If there are outliers in the data (as usually is the case), a single outlier at a few standard deviations from the mean can strongly perturb the fit. This happens because of the sensitivity of the estimator (2-norm of the residuals vector) to extreme outliers which may reflect a true signal as well as statistical flukes. In the latter case, using a 1-norm minimization has been proposed, but it underperforms when occasional outliers betray a short-term, powerful physical signal.

The previously mentioned simple clipping approach is to perform an initial LS fit, find outliers at $t\sigma$ from the mean (σ is standard deviation of post-fit normalized residuals r , t is a threshold, usually equal to 3) and repeat the fit without those. This is equivalent to minimizing the sum of functions $\psi(r)$, where $\psi(r) = r^2$ for $r < 3\sigma$ and 0 otherwise. Multiple other robust functions were suggested in the statistical literature (Huber 1981), Tukey bisquare being one of the most popular. For small residuals it is identical to the square of residuals (just like in LS method), but it tapers off for more statistically significant residuals according to a smooth weight function. The Tukey bisquare regression estimator reaches the 95% efficiency for normally distributed data at $k = 4.685$, and a breakdown point of 0.5 of the S-estimator

is reached at $k = 1.548$. Numerous popular packages such as R, SciPy for Python, or Matlab, provide prepackaged procedures for fitting a robust regressor with various estimator functions, including Huber, Tukey, and trimmed LS.

3. Control star KIC 3836439 = HIP 93954 = HD 178661

To validate our PCA pre-whitening technique and to test the sensitivity of Kepler astrometry and photometry, we randomly selected the control object HIP 93954 from the list of known eclipsing variables (Slawson et al. 2011). It is also a powerful VIM object confidently detected in all the 17 quarters of the main mission (Makarov & Goldin 2016). Fig. 4 depicts a segment of the SAP light curve (left) and the relative centroid position in row coordinates (right), both data series pre-whitened and cleaned as described in Section 2. The VIM effect is evident from the close similarity of the photometric and astrometric variation.

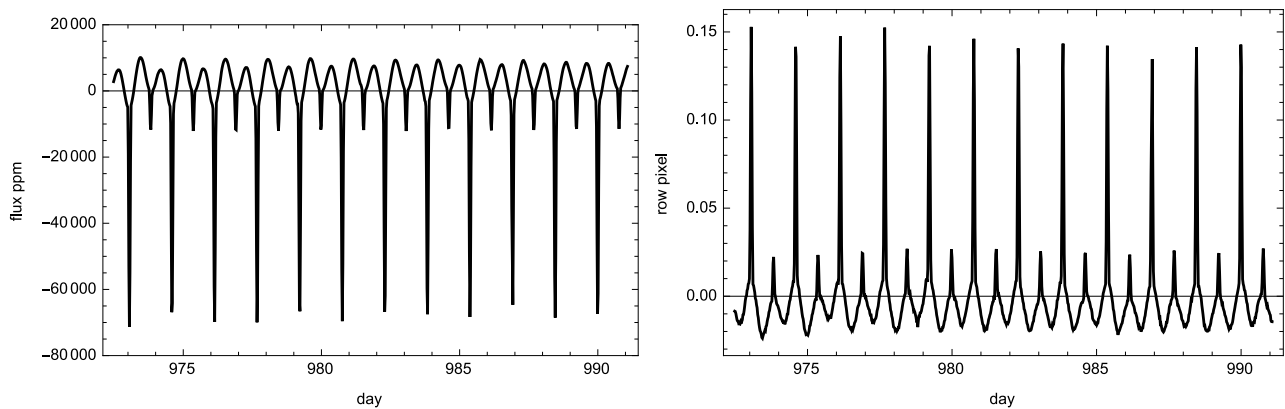


Fig. 4.— PCA-cleaned normalized SAP flux (left) and centroid trajectory of our control star KIC 3836439 for a segment of the main mission data.

First, we note that the pre-whitening procedure has not affected the intrinsic variability pattern of this eclipsing star in either astrometry or photometry but reduced the long-term perturbations. The centroid trajectory looks like a mirror reflection of the light curve. A periodogram analysis performed on both curves confirmed that the main signal resides at a period of 0.77 d, which is half the orbital period as determined by Kepler ($P_{\text{orb}} = 1.5404$ d) and by previous spectroscopic studies. HIP 93954 is a multiple system, at least a triple, with a B companion separated by $1''.31$ from the primary at 1991.25, as determined by Hipparcos (ESA 1997). The separate Tycho-2 photometry for the A and B components is, respectively, $V_T = 7.96$, $B_T - V_T = 0.20$, and $V_T = 9.22$, $B_T - V_T = 0.47$ mag (Fabricius & Makarov 2000). The flux from the primary and the secondary, residing within the same pixel on the Kepler CCD, is totally blended. Both the astrometric and photometric data contain a fair amount of signal from the B component, which is practically unknown.

This star is also listed in the UrHip catalog (Frouard et al. 2015) with a proper motion

which is statistically different from the short-term proper motion determined by Hipparcos. This likely indicates a measurable astrometric orbital motion at the level of a few mas yr⁻¹. Are our PCA-cleaned centroid trajectories good enough to detect the orbital motion directly? To separate the astrometric signals related to VIM from other, possibly intrinsic, astrometric changes, we performed the following modeling of data. If \mathbf{f} is the PCA-cleaned light curve (flux), \mathbf{x} is the centroid coordinate on the same time cadence \mathbf{t} , the linear model for \mathbf{x} is obtained by solving the Least-Squares problem

$$[\mathbf{1} (\mathbf{f} - f_0)/\mathbf{f}] \mathbf{a} = \mathbf{x}, \quad (4)$$

where f_0 is the mean flux outside of the photometric event (quiescent total flux). A fit $\hat{\mathbf{x}}$ can be obtained for a quarter (~ 90 days) or a smaller segment of data. We are interested in the residuals $\mathbf{x} - \hat{\mathbf{x}}$ which should be clean of the powerful correlated VIM signals. Fig. 5 shows modeled residuals for the column coordinates for an entire quarter of the mission. Here we achieved a significant reduction of astrometric variations to small fractions of one milli-pixel. The residual trajectory is very flat and has a sample standard deviation of 0.34 mas in sky angle units. However, the actual single measurement error of thus processed Kepler astrometry is even smaller than that value. Part of the residual variation appears to have a non-stochastic pattern with an amplitude of 0.4 mas and a period of roughly 25 d. This may be first evidence of another hidden orbiting component of the system, which causes the photocenter of the eclipsing pair to shift by 0.4 mas, corresponding to ~ 0.05 AU at the known trigonometric distance. But the more likely explanation for the found patterns in the residual trajectory is another VIM signal, not related to the eclipses of the primary, coming from another blended source. This possibility is supported by the distinctly present high-frequency variation with a period of approximately 0.5 d, typical of giant stars and δ -Sct-type variables. Unfortunately, there seems to be no way to confirm the existence of yet another orbiting companion just with the data in hand.

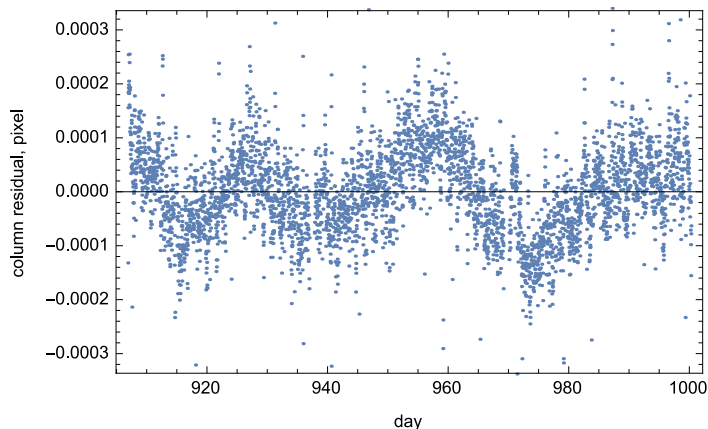


Fig. 5.— Residual centroid trajectory of the control star KIC 3836439 after fitting out the correlated VIM effects (see text).

4. Photometric and astrometric events

Returning to the object of our investigation KIC 8462852, a few major dips detected in the 17 quarterly long-cadence light curves are listed in Table 1. Two events, the first on day 793 and the second on day 1519, stand out due to their surprising amplitudes of ~ 20 and $\sim 15\%$, respectively. The amplitudes of other dips range between ~ 1000 and ~ 70000 ppm. The timing of these events does not seem to be commensurate with any periodic occultation, invalidating the eclipsing binary hypothesis. Some of the dips, but not all, seems to be preceded and followed by smaller amplitude brightening events. The first order of business is to determine if these signals come from the intended target or from a blended source. In our case, the star KIC 8462852 has at least three known relatively close companions.

4.1. Blended companions

The closest known companion was resolved by Keck AO imaging at 2 arcsec due east of the target. It is fainter by 3.8 mag in the NIR H band (Boyajian et al. 2016). Because of the small angular separation and large magnitude difference, this star (called E-companion) is not listed in any major catalog. Regular large-scale images reveal several more distant, but also faint, companions. The most significant neighbors are a star approximately north of the target separated by 9 arcsec from it (we will call it N-companion) and fainter by 5.4 mag in J , and another star 6 arcsec from the N-companion with a magnitude difference of $\Delta J = 5.6$ mag. Both these faint neighbors are listed in the major catalogs, including the 2MASS (Cutri et al. 2003) as 20061551+4427330 and 20061594+4427365, respectively. There is another somewhat fainter companion approximately at position angle 150° , separation 6 arcsec from the target, not named or listed in any of the major astrometric catalogs. All these chance companions, as well as a few even fainter neighbors, are at least partially blended with the target in the digital aperture of KIC 8462852.

The largest degree of flux blending occurs for the closest known neighbor E. Up to 3% of the recorded flux may be coming from this neighbor, and up to 0.6% of light is coming from the N-companion and other neighbors. Obviously, the largest dips of 15% and 20% of the total flux could not originate from any of the neighbors even in the event of their complete occultation. The more numerous smaller dips and other photometric features in the observed light curve could in principle be coming from the blended neighbors, a possibility that should not be outright dismissed.

4.2. VIMs

Comparing the PCA-cleaned light curve of KIC 8462852 in Q8 (Fig. 2) with the PCA-cleaned centroid trajectories for the same quarter (Fig. 3) we immediately see that the target

displays VIM effects. The 15% drop in flux is mirrored by similarly shaped dips in both coordinates on the detector CCD, x (column) and y (row). In this case, we know that the photometric event happened on the target star, KIC 8462852. The moment-based photometer shifted because of the dimmed light from the brightest component. As explained in (Makarov & Goldin 2016), the VIM data can be used to estimate the position angle of the main blended component, but not the separation. The relevant approximate formula for the separation s is

$$s \approx - \left[\frac{\Delta s}{\Delta f} f \right] \frac{f + \Delta f}{f_2}, \quad (5)$$

where f is the total observed flux outside the photometric event (e.g., the median flux in the “quiescent” state), f_2 is the flux of the blended “constant” component, and $\Delta s/\Delta f$ is approximately equal (for small flux variation) to the measurable parameter ds/df called VIM speed, which is the ratio of the astrometric excursion magnitude to that of the corresponding photometric excursion. For the Q8 event, the VIM speed is very small, because a 15% photometric dip ($df/f \approx 0.15$) caused an astrometric perturbation of just a few thousandths of a pixel on the CCD. It is owing to the outstanding single measurement precision of Kepler astrometry (with a standard deviation of ~ 0.8 mas on the sky) that such tiny signals can be confidently detected at all. The separation, however, remains ambiguous because we do not know the fraction of light from the unperturbed companion. But useful estimates can be obtained for the known companions with the available order-of-magnitude knowledge of the flux ratio f/f_2 .

Fig. 6 gives a zoomed-in view of the astrometric trajectories around the photometric dip on day 793 (dots) superimposed with the observed light curve (solid line), which was rescaled and normalized to achieve the best match. The degree of conformity between the astrometric and photometric signals during the 15% dip in flux is remarkable. The normalization coefficient applied to the light curve yields the VIM speed, estimated at -7.9×10^{-8} pix/(e s $^{-1}$) for columns and -9.2×10^{-8} pix/(e s $^{-1}$) for rows of the CCD 56. The VIM speed magnitude is thus 1.2×10^{-7} pix/(e s $^{-1}$) in the direction 229° on the CCD. With a median flux of 2.4×10^5 e s $^{-1}$, the coefficient in the square brackets in Eq. 5 amounts to 2.9×10^{-2} pixels. The closest companion E is at $2'' = 0.5$ pixels. Hence, the estimated ratio f/f_2 is roughly 17, if companion E is responsible for the VIM. This number seems to be small given the magnitude difference $\Delta H = 3.8$ mag, unless companion E is a blue star. On the other hand, the closest neighbor may not be the dominating VIM companion, because the VIM speed, which defines the magnitude of the astrometric signal, is proportional to the separation. Somewhat counter-intuitively, a more distant neighbor may cause a greater VIM as long as a significant fraction of its flux falls within the aperture. Furthermore, a distant bright star situated outside the aperture may still be responsible for the largest VIM even when only a small fraction of its flux falls within the aperture, because of a different distribution of light in the extended wings of the image (in which case Eq. 5 is not applicable).

Using the WCS constants and the pixel scale parameters specified in the metadata of the long-cadence FITS files, we transform the VIM direction (229°) in the column-row pixel coordinates into the conventional position angle on the sky, reckoned counterclockwise from

Table 1: Photometric dips in the light curve of KIC 8462852 .

Day	Amplitude ppm	VIM?	Notes
140	4000	yes	brightening before and after event by +1000 ppm
215	1000		modulation in row pixels
260	6000	yes	possible brightening after eclipse
377	1800	?	
427	2100		
502	1200		narrow dip, no obvious brightening before or after
610	2400	yes	not an eclipse but a sudden drop, instrumental effect?
660	1000		broad, shallow dip, complex variability in this quarter
793	150000	yes	no obvious brightening before or after
1144	1000		jitters around probably of instrumental nature
1206	4000	yes	narrow, well defined event
1519	204000	yes	most prominent event
1540	25200	yes	bracketed by brightening events, VIM speed is clearly different
1568	74500	yes	bracketed by brightening events

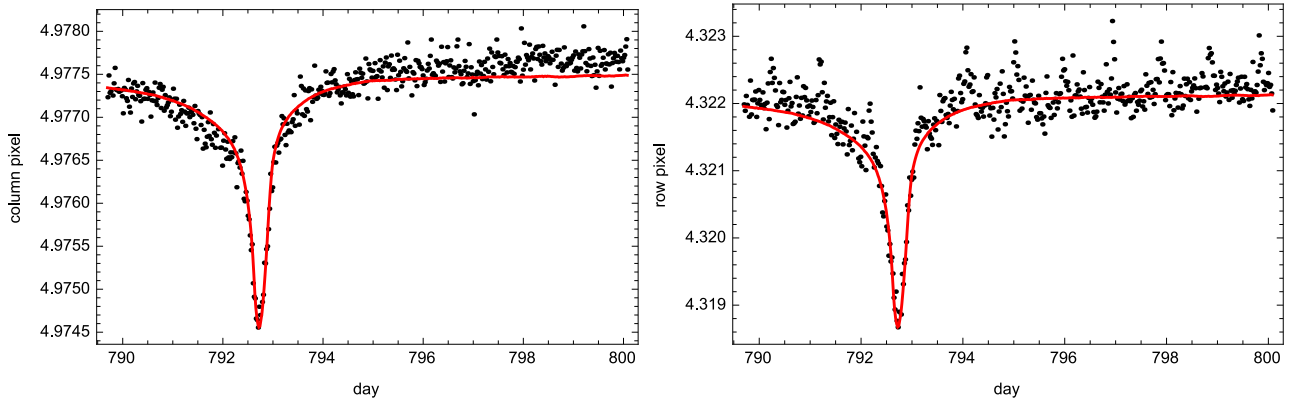


Fig. 6.— PCA-cleaned centroid trajectories of KIC 8462852 in Quarter 8 in column (left) and row (right) pixel coordinates around the major photometric event on day 1519, marked with dots. The superimposed solid curves represent the normalized and rescaled flux observed on the same cadence.

north through east. This transformation yields a PA= 336° with an uncertainty of about $\pm 10^\circ$. This direction does not match any of the previously discussed close companions. However, an interesting star is located at a larger distance from the target, viz., $36''$, PA= 344° . It is listed in several major catalogs, including 2MASS as 20061453+4428001. The star with a $V \approx 15.5$ mag is optically fainter than its neighbor KIC 8462852 by 3.6 mag, but the 2MASS magnitudes $J = 10.577$, $H = 9.455$, $K_s = 9.075$ indicate that it is exceptionally red and in fact brighter in the infrared. Little is known about this star apart from the NIR and MIR magnitudes and proper motion (which is small and unremarkable). The J2000 ICRS coordinates of the star are RA = 301.560574° , Dec= $+44.466687^\circ$ in the URAT1 catalog (Zacharias et al. 2015).

One may wonder why this distant and faint companion produces the weak, but measurable, VIM effects while the closer neighbor KIC 8462860, discussed by Montet & Simon (2016) as a likely contamination source, does not? KIC 8462860 is also 3.65 mag fainter than our target star, separated by 25 arcsec at PA= $\simeq 20^\circ$. One possible explanation would be that the bloated and strongly asymmetric PSF in this corner of the Kepler field of view, depicted in Fig. 1 of (Montet & Simon 2016), picks up more photons from the sources in specific directions on the CCD. However, we will see that the VIM direction of the major events is consistent between the mission quarters, where the orientation of the CCD and the PSF was different on the sky. This interpretation meets significant difficulties, leaving room for a very close, yet unresolved, companion.

Speculatively, if the weak VIM signals are caused by a very close unresolved companion, it should be very close to the target star, and also rather faint. Given the limits of the high-resolution imaging and speckle interferometry from (Boyajian et al. 2016), it should be either closer than ~ 40 mas, or have a delta magnitude above 4. Furthermore, it should be an optical companion given the absence of radial velocity variations, i.e., a chance projection on the sky of an unrelated star. The probability of such projections is quite low, of order two parts in 10 000. But between the 170 000 Kepler targets, there should be a few dozens such alignments. Some of these alignments are bound to include foreground companions. This may give some more credibility to the hypothesis of chance occultations by foreground objects presented in Section 6.

The major event on day 1519 took place in Q16, almost exactly two years after the 15% dip on day 793. The Kepler telescope observed the same area of the sky in four different and fixed orientation states (roll angle). Each orientation state was strictly repeated in a one-year cycle. Therefore, the target was observed in Q16 with the same orientation of the telescope, and in fact, on the same pixels, as in Q8. We therefore expect to find a VIM effect similar in direction and magnitude to the one on day 793. The observational data thwart this expectation and provide additional puzzles.

Fig. 7 displays a zoomed-in portion of the astrometric data (black dots, left plot for x and right for y) superimposed with the appropriately shifted and scaled light curve (solid line). The main dip is split, with a smaller component preceding the larger one by some 18 hours. Both components are reproduced in the centroid trajectory, but apparently not as closely as in Fig.

6. The estimated VIM speed is -1.3×10^{-8} pix/(e s⁻¹) for columns and -3.1×10^{-8} pix/(e s⁻¹) for rows, with a magnitude of 3.4×10^{-8} pix/(e s⁻¹) and a position angle of 247° on the detector. Even though the direction is roughly the same as in Q8, the magnitude of VIM is smaller by a factor of 3.5. The observed nonlinear character of these VIM effects may be explained by the influence of a very distant, but bright neighbor. The brightest companion at large is the rather unremarkable red giant star KIC 8462934 ($V = 11.51$ mag) separated by 89 arcsec, which was investigated for asteroseismology (Pinsonneault et al. 2014) but does not exhibit any unusual variability. The detected VIM speed in Q16 can be significantly different with the same configuration of blended images, if the light distribution of the portion coming from the distant neighbor has a significant gradient, and the position of the aperture with respect to the pixel grid is slightly shifted with respect to that in Q8. Alternatively, we may conclude that the astrometric excursion is capped at approximately 12 mas on the sky, no matter how deep the underlying photometric variation is. This explanation would be consistent with the unresolved optical companion hypothesis.

Fig. 7 provides an even greater puzzle outside of the main event 1519. We can clearly see a dip in both coordinates on day 1517, which barely registers in the re-scaled light curve. The excursion is larger in the column direction, where it is comparable in magnitude to the main VIM effect, but the observed total flux hardly changed at that time. This implies that the VIM speed of this event is more than 10 times greater than the VIM speed of the main photometric event, and the direction is somewhat different too. How can the VIM speed be so different for two close VIM occurrences with a fixed configuration of stars? Eq. 5 implies that the VIM speed is proportional to f_2/f , where f_2 is the flux from the photometrically constant companion. If a much fainter companion is dimmed while the bright target star remains constant, the ratio f_2/f is close to unity, and the VIM speed can be greater by orders of magnitude even for the same pair of blended images. In other words, the VIM speed is extremely sensitive to whether the photometric change happens on the bright or the faint companion. The conclusion is that the VIM on day 1517 was caused by a photometric variability of *another* star.

Given these observations, we begin to suspect that the seemingly disorderly collection of photometric dips is coming from different sources overlapping with the aperture footprint.

4.3. The origin of small-amplitude dips

The smaller dips in the light curve at a few to several thousands ppm observed across the mission time span are sometimes associated with marginally small excursions in centroid position (Table 1). These barely detectable VIM effects require a more sophisticated method of analysis than the previously used rescaling and amplitude matching. The astrometric trajectories are especially difficult to analyze for small-amplitude wobbles because of the presence of larger perturbations on similar or longer timescales. We focus in this paper on two medium-sized events on days 140 (Q1) and 260 (Q3), which are the most distant in time from the two major events at the end of the mission.

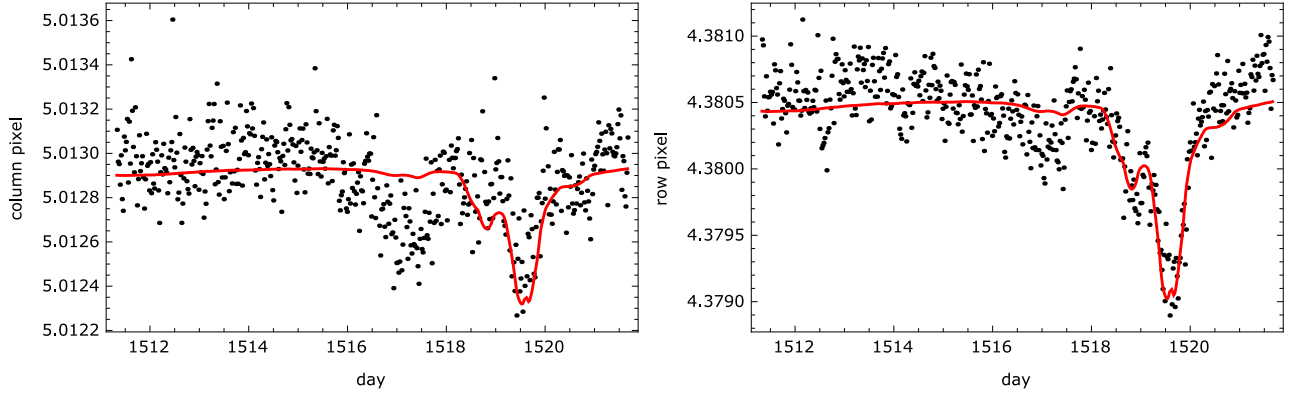


Fig. 7.— PCA-cleaned centroid trajectories of KIC 8462852 in Quarter 16 in column (left) and row (right) pixel coordinates around the major photometric event on day 1519, marked with dots. The superimposed solid curves represent the normalized and rescaled flux observed on the same cadence.

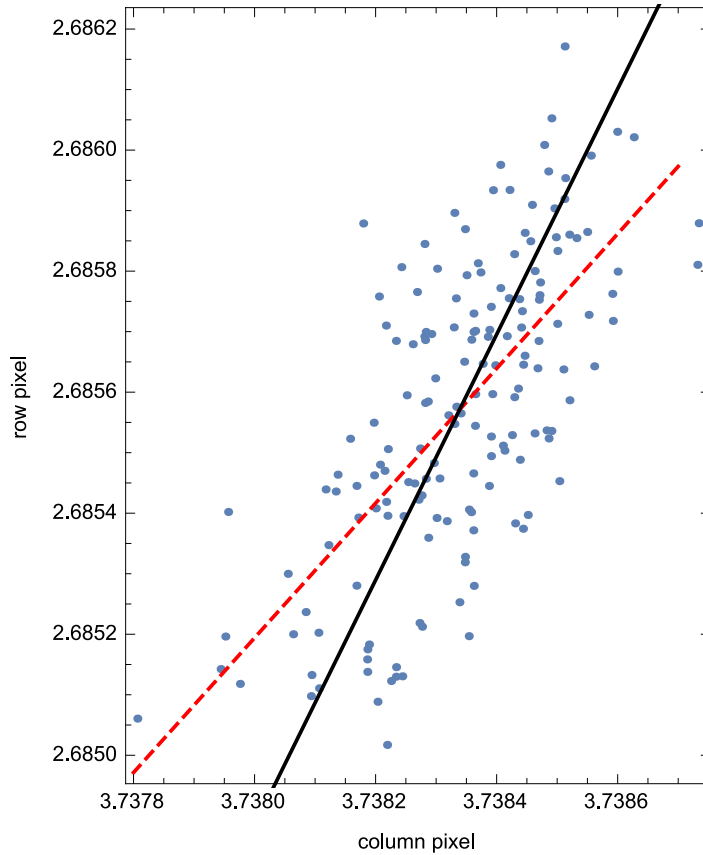


Fig. 8.— The segment of the VIM trajectory in detector's pixel coordinates caused by the small-amplitude photometric event on day 260 in Q3. The regular least-squares fit is shown with a dashed line; the more accurate orthogonal distance regression is shown with a solid line.

For each of these VIM events, we select time boundaries corresponding to the beginning and the end of the flux dip. For example, for the first event, the interval is [138.3, 143.6] days. We use only the PCA-cleaned data within these intervals. If we plot coordinate measurements versus simultaneous flux measurements, a correlated VIM shows up as a linear dependence with a slope indicating the VIM speed ds/sf . If we plot y -coordinates versus x -coordinates for the same cadence of measurements, the slope of a linear trend indicates the direction of the correlated 2D motion, i.e., the VIM direction. Fig. 8 shows the y versus x plot for the stronger and more discernible VIM on day 260. The next step is to fit a straight line to this cloud of points. The regular least-squares linear regression, shown with the dashed line in the plot, provides a poor fit in this case strongly underestimating the slope. This is because the least-squares (LS) method is designed to minimize the quadratic sum of residuals in the fitted variable (y), while the argument values (x) are implicitly assumed to be precise. In our case, both coordinate measurements are perturbed by random errors. The more appropriate method of fitting is the orthogonal distance regression, described in many statistical textbooks. The simplest algorithm in implementation is the total LS, which allows to fit 2D data sets of inhomogeneous precision and to employ elements of robust statistical estimation (including Tukey bisquare estimator) via appropriate weighting of data points, but it performs only the 2-norm optimization. The solid line in Fig. 8 shows thus obtained total least-squares fit assuming the same error in x and y . Visually, it provides a much more realistic fit given uncertainties in both coordinates. We also tried a generalization of the orthogonal distance regression adapted to the 1-norm solution (i.e., minimizing the absolute values of weighted residuals in both coordinates), but found the results close to the total LS fit.

Using the appropriate WCS constants given in the metadata, we estimate the VIM directions at 336° for Q1 and 329° for Q3. These position angles are consistent, within the expected errors, with the estimated directions of the two major events (Section 4.2). The most plausible interpretation is that the same faint companion, possibly 2MASS 20061453+4428001, is mostly responsible for the observed VIM and the dimming occurs on the target star KIC 8462852. Indeed, if the dimming belongs to the companion, the photocenter should move in the opposite direction. The VIM speed magnitude, on the other hand, is less consistent with this scenario. The estimated values are 3.6×10^{-7} pix/(e s⁻¹) in Q1 and 1.4×10^{-7} pix/(e s⁻¹) in Q3. The observed scatter in VIM speed between individual events is hard to explain. In particular, the estimated VIM speed for the major event on day 1519 is roughly 10 times smaller than that for the much smaller dip on day 260. It appears that no matter how large the photometric changes are, the astrometric excursion is upper-limited to ~ 12 mas on the sky. If this is true, the only possible explanation is that there is an unresolved companion at a comparably small separation.

4.4. Medium-amplitude photometric events

To complete our VIM analysis, we analyze two medium-amplitude photometric dips that occurred on day 1540 (Q16), or some 20 days after the greatest event, and day 1568 (Q17). Fig. 9 shows the portions of the PCA-cleaned light curve centered on these two events. Unlike the two major dips in Q8 (Fig. 6) and Q16 (Fig. 7), with fairly smooth ingress and egress, both variations in question are marked by pronounced brightening preceding and following the dip. We applied the algorithm described in Section 4.3 to both medium-amplitude events to determine the VIM parameters

The day 1540 dip in Q16 is studied by using the astrometric and photometric measurements between days 1539 and 1541. An orthogonal distance regression yields a $y(x)$ slope of 1.564. The corresponding position angle on the sky is 328° . From $x(f)$ and $y(f)$ fits, we derive a VIM speed of 2.6×10^{-7} pix/(e s $^{-1}$), which is in the range of small-amplitude events, but significantly greater than the VIM speed of the major events. The day 1568 event took place roughly between days 1567 and 1570. The position angle is estimated at 322° , and the VIM speed is approximately 1.2×10^{-7} pix/(e s $^{-1}$).

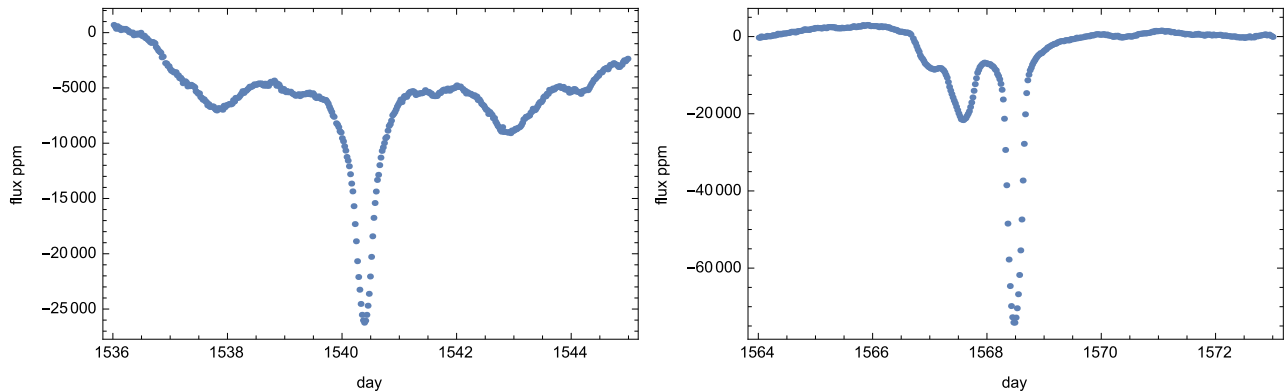


Fig. 9.— PCA-cleaned light curves around the medium-amplitude photometric events on day 1540 in Q16 (left) and day 1568 in Q17 (right).

The six photometric dips we analyzed in detail for VIM effects vary in amplitude from 4000 to 204000 ppm, but they all have consistent direction on the sky, $PA = 330^\circ \pm 6^\circ$. This points at one of the several faint companions of the target star as the dominant source of astrometric perturbation when the target flux changes. The VIM speed, indirectly related to the separation between the companions and their relative brightness, varies between the events in a wide range, displaying a nonlinear dependence on the amplitude. It seems that the larger photometric dips cause relatively weaker astrometric excursions. The most prominent VIM companion is outside the range of quasi-linear blending of signals, i.e., it is probably closer to the boundary of the digital aperture, or, on the contrary, very close to the target star. Some powerful astrometric perturbations barely noticeable in the light curves are also present in the data.

5. Periodogram analysis

Boyajian et al. (2016) discuss a significant periodical signal detected in the light curve of KIC 8462852 with a period of 0.88 d. They do not mention that this periodicity is also present in the astrometric positions of the target. It is obvious, for example, in Fig. 6 outside of the main event, especially in the row coordinate (right plot). The shape of the periodic variations is sharp-crested, which simply reflects the shape of light curve variations. The 0.88-day flux periodicity is relatively weak but still confidently detectable in our Lomb’s χ^2 periodogram analysis, as we will see in the following.

We use the algorithm described by Makarov et al. (2012), developed for exoplanet search in astrometric and radial velocity data. The algorithm is based on simple and mathematically rigorous principles, incorporating elements of robust statistical analysis. In this application, we are using only the first part of the algorithm, namely, the periodogram analysis. A periodogram is a function $A(P)$ where P is the fitting sinusoid period for a given time series of data \mathbf{d} (not necessarily equally spaced) measured at times \mathbf{t} , and A is the amplitude of the fitting sinusoid. The method proposed by Lomb (1976) is to solve the system of linear equations

$$[\mathbf{1} \cos(2\pi\mathbf{t}/P) \sin(2\pi\mathbf{t}/P)] \mathbf{a} = \mathbf{d} \quad (6)$$

by the LS method (possibly introducing weights for measurements of unequal precision) for each trial period P . The sought amplitude is then $A = \sqrt{a_2^2 + a_3^2}$. Alternatively, the objective function can be the χ^2 of post-fit residuals. The amplitude periodogram (with peaks indicating significant periodic signals) and the χ^2 periodogram (with dips indicating significant periodic signals) are practically identical as far as the amount of information is concerned, but the latter is more amenable to the confidence (or false alarm probability) estimation by the standard F -test.

We applied this periodogram analysis to the PCA-filtered flux and astrometric time series of KIC 8462852 for each quarter of the mission. The purpose was to identify significant periodic signals. In the range of periods between 5 and 90 days, the light curves often include significant periodicities with amplitudes of 100 to 200 ppm. However, these signals appear to be transient, as neither phase nor period is stable between the quarters. For example, the highest peak in the $A(P)$ curve rising up to 107 ppm is found at $P = 19.7$ d for Q11, but in the next quarter Q12, the most prominent period is 44 d (although a slightly smaller peak is present at $P = 18.5$ d). Such shifting, unstable periodicity is typical for normal, magnetically inactive and slowly rotating stars, such as the Sun. However, this surmise contradicts the high projected velocity of rotation determined by Boyajian et al. (2016). The possibility that the transient periodicities found in this range are artifacts caused by the PCA pre-whitening can not be ruled out at this stage. Indeed, some of the principal components shown in Fig. 1, look sinusoid-like. As a way to resolve this problem, one could perform a separate periodogram analysis of each of the 4 principle components for each quarter and take into account the corresponding coefficients of the Tukey bisquare fit. We have not performed this analysis because the results seem to be negative in any case.

At periods shorter than 5 d, the dominating periodic signal invariably comes at $P = 0.88$ d. This periodicity was already detected and discussed by Boyajian et al. (2016), who interpreted it as rotation of the target star. Our calculations with PCA pre-whitened light curves confirm the presence of this signal. For individual quarters, the amplitude of the main sinusoidal term is 50 – 218 ppm. The signal is definitely non-sinusoidal, which is betrayed by a series of harmonics at one half, one third, etc., the main period. Visually, the 0.88-day variation in flux is sharp-crested, rather than flat, at the bottom, and resembles the light curves of short-period eclipsing binaries or rotating ellipsoidal stars. It does not look like a small-amplitude variation caused by transient and short-lived spots on the rotating surface (Makarov et al. 2009).

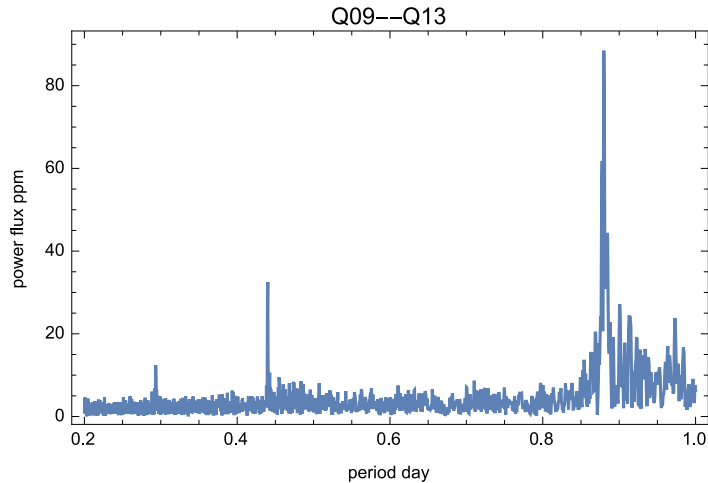


Fig. 10.— Lomb’s periodogram of the combined light curve for KIC 8462852 over 6 quarters, Q9 – Q15. The strong peak at $P = 0.88$ d and its harmonics (not shown in this graph) indicates that the phase of this periodic variation was stable over at least 1.5 years of continuous observation.

On the Sun, photospheric spots, plages, and other magnetic features appear with the same probability at any longitude and very seldom last for longer than one revolution period. The phase of rotation-induced variations in the solar irradiance curve is therefore scrambled on timescales longer than one month. Even the most magnetically active stars with much greater amplitudes of variability do not keep the same phase of variation longer than a few months, unless their activity is enhanced by a close binary companion. On the other hand, F-type stars have shorter periods of rotation and more persistent photometric features. Mathur et al. (2014) investigated the light curves of 22 F-type stars with periods between 2 and 12 days and found a group of 5 stars with modulations which remained coherent in phase over the entire duration of observation. They interpreted these stars as rotators with very stable active longitudes where groups of starspots predominantly emerge. Mathur et al. (2014) discarded the possibility of stable classical pulsations because the stars are not residing in the known instability zones. The morphology of the 0.88 d variations in the light curve, which are flat at the top and sharp at the bottom, also favor the rotational modulation interpretation.

Non-radial pulsations caused by interior acoustic waves are unlikely to keep a permanent

phase for long durations of time. As a way to probe for the origin of the 0.88-day signal, we computed a periodogram for a combined light curve over five quarters, Q9 through Q13. This stretch represents a quiescent interval without major photometric peculiarities. The resulting amplitude periodogram is shown in Fig. 10. The 0.88-day peak is very sharp and strong, as well as the second and third harmonics of the main mode. If the phase of this variation changed during this 15-month interval, the peak would be diluted or completely gone, because we fit a single pair of sine and cosine functions to the entire data set. Thus, the periodic signal is remarkably persistent over 15 months at least.

A significant fraction of field F-type stars possess elevated degrees of coronal magnetic activity, as betrayed by intense X-ray radiation (Suchkov et al. 2003). Those active F stars include young stars, binaries of RS CVn and BY Dra-type, and old, slightly evolved stars of unclear nature. Young stars of pre-main sequence age and components of tight binaries are known to rotate fast, which is the reason for their elevated X-ray activity. Our object of investigation, however, is neither young or binary, nor is it associated with a detectable X-ray source. Here we will argue that this signal comes from one of the blended companions rather than from KIC 8462852.

We estimated a VIM speed of $10^{-8} - 10^{-7}$ pix/(e s⁻¹) for the major photometric events, which definitely happened on the target star simply because of the large magnitude of variation (Sect. 4). The amplitude of the 0.88-day signal is 90 ppm (Fig. 10), which is approximately 22 e s⁻¹. The expected amplitude of a VIM in the astrometric trajectory is then of order $10^{-6} - 10^{-5}$ pix. This is too small to be detected in the Kepler data. However, the 0.88-day periodicity is clearly present in the astrometric data, and *sometimes*, its magnitude is quite large, for example, see the right plot in Fig. 6 for Q8 outside of the major dip on day 793, where its amplitude is up to 10^{-3} pix. Thus, the VIM caused by the 0.88-day periodicity is 100 – 1000 times stronger in VIM speed than the main event. Furthermore, as Fig. 11 shows, the VIM in row pixel coordinates is counter to the flux variation, whereas they are aligned for the dip. The VIM direction is almost opposite to the excursion caused by the dip. We detect two distinct VIM events simultaneously perturbing the data, which originate from different sources.

6. A swarm of comets or interstellar junk?

Bodman & Quillen (2016) argued that a single comet can not produce a dip in the light curve as deep and as long as the two major events observed in Q8 and Q16. They propose that a swarm of at least 30 comets traveling in a tight pack can explain the events during the two last quarters, Q16 and Q17. The dip in Q8 can not be explained by the same swarm of objects, however. This interpretation invokes multiple groups of comets in significantly different orbits around the star, speculatively indicating the start of a Late Heavy Bombardment episode.

We propose a different interpretation which is consistent with the observed peculiarities of

the Kepler data and other information about the star. We consider a large swarm of interstellar objects ranging in size from small comets to planetoids unrelated to the target star, traveling in the interstellar space, which happened to cross the line of site to the target and, perhaps, its near neighbors on the sky. The irregularly spaced events are explained as randomly timed occultations from different parts of the swarm. Such free-traveling swarms can be the remnants of catastrophic disintegration of a rich exoplanetary system or a star-formation episode in a depleted molecular cloud. The interstellar Na D absorption lines detected by Boyajian et al. (2016) are likely to be related to the foreground cloud. The existence of interstellar comets has been suspected for some time but no direct evidence has yet been found. Alternatively, a swarm of comets orbiting another foreground star which accidentally happened to be close to the target star in the sky projection (an optical pair) can also be considered.

What kind of density should a swarm of comet-like or planetoid-like objects have to produce the observed rate of irregular occultations? Assuming a radius of $1.7 R_{\odot}$ for KIC 8462852 (Huber et al. 2014) and a distance of 500 pc to the star, the cross-section of the occultation events during the 4 years of Kepler main mission is $0.125 \times 10^{-6} \mu$ in arcsec², where μ is the relative proper motion of the swarm and the target star in mas yr⁻¹. The expected number of occultation events is, approximately,

$$N \approx 10^{-3} \left[\frac{5D_j}{D_s} \right]^2 \left[\frac{\rho}{\text{AU}^{-2}} \right] \left[\frac{\mu}{1 \text{ mas yr}^{-2}} \right] \quad (7)$$

where D_s is the distance to the star and D_j is the distance to the foreground swarm. Since the relative proper motion is expected to be of order 10 mas yr⁻¹, a surface density of 1000 per AU² is sufficient to produce the observed number of events at a distance ratio of 5, which is further relaxed to ~ 40 if the swarm is close to the target star. Such surface densities are probably feasible, considering, for example, the approximate volume density 10^5 AU^{-3} of asteroids larger than 1 km in diameter in the Solar asteroid belt.

The relative proper motion can be estimated assuming a distance of 500 pc and a typical duration of occultation of 1 d. The upper limit is 6 mas yr⁻¹, which is a small number considering that the proper motion of the star itself is greater than 10 mas yr⁻¹. The distance estimation for KIC 8462852 is quite uncertain, however. Ammons et al. (2006) estimates a much lower photometric distance of 32 pc, and a lower $T_{\text{eff}} = 5916 \text{ K}$, which is more consistent with the colors determined in the AAVSO photometric survey (Henden et al. 2016), $B - V = 0.508 \pm 0.062$, $g' - r' = 0.35 \pm 0.06 \text{ mag}$. A smaller distance to the star implies a higher relative proper motion.

A cloud of foreground comets, whether solivagant (traveling by themselves) or attached to a foreground star, analogous to our system’s Kuiper belt, could explain the irregular arrival of occulters, the varying depth and duration of observed dips, and the magnitude of these events. Giant comets are no longer required, as a closer body of regular size obstructs more light from the target star.

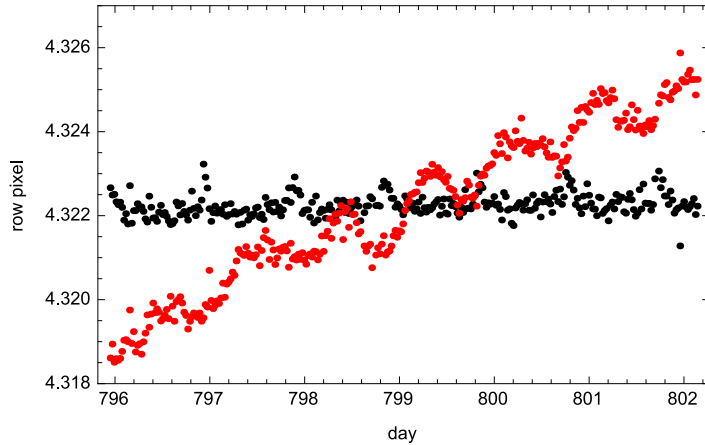


Fig. 11.— Original (unprocessed) SAP data collected during Q8 of the mission. Black dots represent individual row (2nd coordinate) pixel coordinates, red dots show the flux measurements rescaled to fit the same range of values as the coordinates.

7. Summary

The complex pattern of photometric variability detected for KIC 8462852 is often, but not always, faithfully reflected in correlated astrometric excursions called VIM. This confirms a non-negligible amount of blending in the detected aperture flux. While most of the prominent dips in the light curve and the corresponding VIM events indicate a single direction to the largest perturbing component ($PA \approx 330^\circ$), proving that they occur on the intended target, the magnitude of astrometric perturbations shows a large scatter and a nonlinear dependence on the photometric amplitude. A very close unresolved companion is possible. An alternative explanation is a distant ($\gtrsim 20''$) but brighter companion. A number of VIM events, however, have much greater VIM speeds and different directions. These are caused by photometric events on the faint optical companions of the target. The small-scale variability observed outside of the main dips may be caused by the blended signals.

The most remarkable 0.88 d variability previously attributed to KIC 8462852, appears to be coming from a contaminant, but not from the same companion as the most pronounced VIMs. Per Eq. 5, the observed VIM speed (ds/df) is very sensitive to the origin of photometric variability when two star images are blended. If the variability occurs on the faint companion, the VIM speed is much greater and the VIM direction is roughly opposite to the main events. The phase (but not the observed amplitude) of this non-sinusoidal wave is found to be remarkably stable over at least 15 months of continuous data. The possible origin of this signal is synchronous rotation of an optical companion, unrelated to the target star. Transient periodicity occurs in both light curve and astrometry at longer periods of 10 – 40 d, but it is not not persistent in phase, amplitude, or frequency.

The observed pattern of stochastic, randomly spaced photometric events and the complex character of VIM interference point at a foreground swarm of comet-like objects or planetesi-

mals as a more plausible interpretation than a family of highly eccentric comets orbiting the target star. The swarm may be a free-traveling interstellar group of objects or a belt associated with the hypothetical optical companion.

REFERENCES

- Ammons, S.M., Robinson, S.E., Strader, G., et al. 2006, *ApJ*, 638, 1004
- Abeyssekara, A.U., Archambault, S., Archer, A., et al. 2016, *ApJ*, 818, 33
- Boyajian, T.S., LaCourse, D.M., Rappaport, S.A., et al. 2016, *MNRAS*, 457, 3988
- Christiansen, J.L., Jenkins, J.M., Caldwell, D.A., et al. 2012, *PASP*, 124, 1279
- Bodman, E.H.L., Quillen, A. 2016, *ApJ*, 819, L34
- ESA 1997, *The Hipparcos and Tycho Catalogues*, ESA SP-1200
- Fabrizius, C., Makarov, V.V. 2000, *A&A*, 356, 141
- Frouard, J., Dorland, B.N., Makarov, V.V., et al. 2015, *AJ*, 150, 141
- Henden, A.A., Templeton, M., Terrell, D., et al. 2016, *VizieR Online Data Catalog: AAVSO Photometric All Sky Survey (APASS) DR9*
- Huber, P.J. 1981, *Robust Statistics*, Wiley
- Huber, D., Silva Aguirre, V., Matthews, J.M., et al. 2014, *ApJS*, 211 2
- Cutri, R.M., Skrutskie, M.F., Van Dyk, S., et al. 2003, *The 2MASS All-Sky Catalog of Point Sources*, IPAC/California Institute of Technology
- Golub, G.H., Van Loan, Ch.F. 1983, *Matrix Computations*, The John Hopkins University Press, Baltimore MD
- Lomb, N.R. 1976, *Ap. Space Sci.*, 39.447
- Makarov, V.V., Goldin, A. 2016, *ApJS*, 224, 19
- Makarov, V.V., Beichman, C.A., Catanzarite, J.H., et al. 2009, *ApJ*, 707, L73
- Makarov, V.V., Berghea, C., Efroimsky, M. 2012, *ApJ*, 761, 83
- Marengo, M., Hulsebus, A., Willis, S. 2015, *ApJ*, 814, 15
- Mathur, S., García, R.A., Ballot, J., et al. 2014, *A&A*, 562, A124
- Montet, B.T., Simon, J.D. 2016, arXiv:1608.01316

- Pinsonneault, M.H., Elsworth, Y., Epstein, C., et al. 2014, *ApJS*, 215, 19
- Slawson, R.W., Prša, A., Welsh, W.F, et al. 2011, *AJ*, 142, 160
- Still, M., & Barclay, T. 2012, *Astrophysics Source Code Library*, 1208.004
- Suchkov, A.A., Makarov, V.V., & Voges, W., F. 2003, *ApJ*, 595, 1206
- Thompson, M.A., Scicluna, P., & Kemper, F., et al. 2016, *MNRAS*, 458, 39
- Wright J.T., Carter, K.M.S., Zhao, M., et al. 2016, *ApJ*, 816, 17
- Zacharias, N., Finch, C., Subasavage, J., et al. 2015, *AJ*, 150, 101